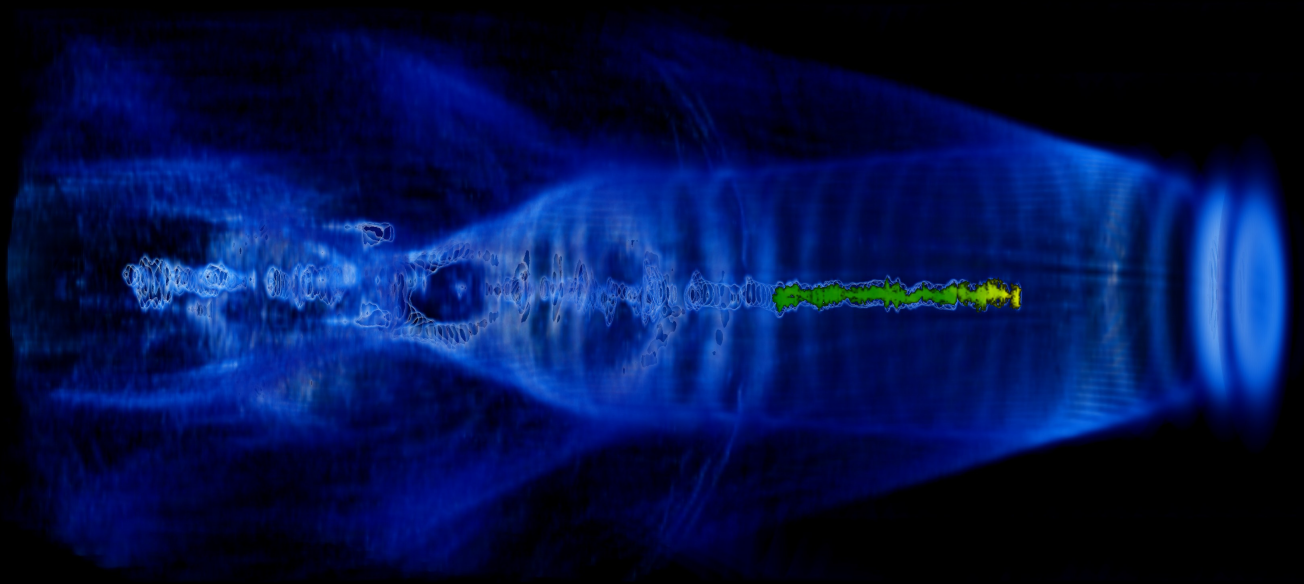


MASTER'S THESIS 2019

A compact plasma beam dump for next generation particle accelerators

OSCAR JAKOBSSON

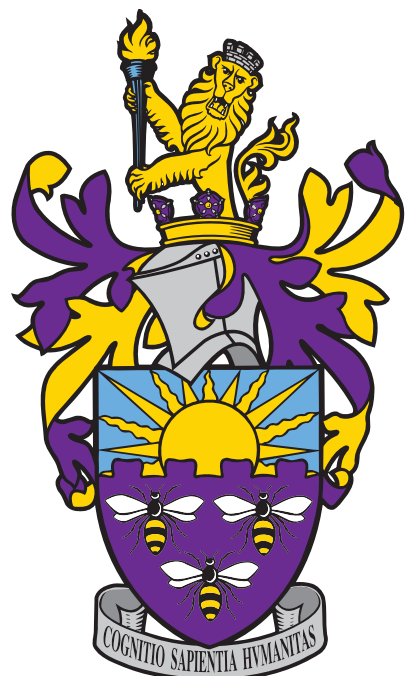


SCHOOL OF PHYSICS AND ASTRONOMY
THE UNIVERSITY OF MANCHESTER



A compact plasma beam dump for next generation particle accelerators

OSCAR JAKOBSSON



School of Physics and Astronomy
Cockcroft Accelerator Group
THE UNIVERSITY OF MANCHESTER
Manchester, United Kingdom 2019

A compact plasma beam dump for next generation particle accelerators
OSCAR JAKOBSSON

© OSCAR JAKOBSSON, 2017.

Supervisor: Guoxing Xia, Cockcroft Accelerator Group

Master's Thesis 2019
School of Physics and Astronomy
Cockcroft Accelerator Group
The University of Manchester

Cover: XXX.

Typeset in L^AT_EX

A compact plasma beam dump for next generation particle accelerators
OSCAR JAKOBSSON
School of Physics and Astronomy
The University of Manchester

Abstract

Keywords: LWFA, PWFA, collective deceleration, plasma beam dump, EuPRAXIA

Acknowledgements

Lorem ipsum dolor sit amet, consectetur adipisicing elit, sed do eiusmod tempor incididunt ut labore et dolore magna aliqua. Ut enim ad minim veniam, quis nostrud exercitation ullamco laboris nisi ut aliquip ex ea commodo consequat. Duis aute irure dolor in reprehenderit in voluptate velit esse cillum dolore eu fugiat nulla pariatur. Excepteur sint occaecat cupidatat non proident, sunt in culpa qui officia deserunt mollit anim id est laborum.

Oscar Jakobsson, Manchester, January 2019

Contents

List of Figures	xi
1 Introduction	1
1.1 Conventional and plasma-wakefield accelerators	1
1.2 Beam dumps	2
1.3 Outline of report	4
2 Simulations	5
2.1 Plasma simulations	5
2.2 EPOCH	5
2.3 Particle-in-Cell Codes	6
2.3.1 Input deck	7
2.3.2 Non-analytical bunch initialisation	7
3 Theoretical foundations	9
3.1 Introduction	9
3.2 Linear fluid model	9
3.2.1 Longitudinal Accelerating Field	11
3.2.2 Transverse Field	14
3.2.3 Collective Plasma Deceleration – Linear regime	17
3.3 Non-linear Regime	18
4 Simulation tests	19
4.1 Plasma deceleration - Uniform density	19
4.2 Larger bunch	20
4.2.1 Transverse instabilities in quasilinear regime	20
4.3 Hybrid Scheme - Feasibility study	20
4.3.1 Initialising a decelerated bunch	20
4.3.2 Introduction of co-propagating laser	20
5 Ongoing and future work	25
6 Conclusion	27
Bibliography	29
A Appendix: Input decks	I

Contents

List of Figures

1.1	Energy distributions of an electron bunch during propagation through a dense plasma, as found by Wu et. al [19]. 1(b) shows non-relativistic particles falling behind the head of the bunch and 1(c) shows their subsequently re-acceleration. The x-axis shows the distance along the bunch in relation to the plasma wavelength, which is covered in chapter 3.	3
1.2	Outline of the hybrid beam dump scheme at five stages. (i) The incoming ultra-relativistic (violet) electron bunch passes through vacuum towards the first plasma cell. (ii) The electron bunch loses energy as it propagates through the plasma. A non-relativistic (red) tail of particles is formed behind the the head of the bunch, which maintains its energy. (iii) The non-relativistic tail is removed by propagating through an absorbing material and the path of the head is bent by magnets so as to be aligned behind a laser pulse. (iv) The laser pulse drives a plasma wakefield in front of the remaining bunch, decelerating it to non-relativistic energies. (v) The remaining energy is absorbed.	4
2.1	The field update and particle push algorithm run b	7
3.1	•	15
3.2	Simulation vs. theory for linear regime with $n_p/n_b = 100$	15
3.3	•	16
3.4	Transverse force - theory vs. simulation	17
4.1	•	20

1

Introduction

1.1 Conventional and plasma-wakefield accelerators

Ultra-relativistic electron beams with single-particle energies in excess of a GeV form an integral part of many areas of contemporary science, industry and medicine. For instance, monoenergetic electron bunches allows for the generation of high-quality X-ray pulses through the use of undulators; a technique by which ultra-relativistic electron bunches are rapidly oscillated back-and-forth perpendicular to their direction of propagation [1]. This oscillatory motion can be tuned to generate highly coherent synchrotron radiation in the X-ray spectrum, which can be used in medicine for advanced tissue diagnostics, tomography and radiotherapy cancer treatments [2]. Operating at higher energies, the 1.7 km long European X-ray free electron laser (XFEL) facility in Hamburg, Germany, employs 17.5 GeV electron bunches to generate extremely intense femtosecond X-ray pulses which are used for fundamental research into the structure of materials, biological molecules and even to generate movies of molecular reactions [1]. Probing even smaller length scales takes us into the realm of high-energy electron-positron collider physics, where the size of accelerators grows accordingly. From the 3.2 km long, 45 GeV, SLAC Linear collider (SLC) at Stanford to the decommissioned 27 km long, 105 GeV, Large Electron Positron collider (LEP) at CERN, the fine details of the smallest constituents of our theories are being explored through tests of the standard model of particle physics. Even higher energy electron-positron colliders such as the proposed 50 km long International Linear Collider (ILC) aims to achieve single-particle energies up to 500 GeV. The reason for these progressively larger accelerators stems in part from the reliance on resonant radiofrequency (RF) cavities in order to accelerate particles, which are currently limited to sustaining electric fields no larger than 100MV/m, beyond which point further increase is hampered by material breakdown of the inner walls of the cavity [3]. As the demand for high-energy particle accelerators grows in medicine, industry and fundamental research, the size and cost of accelerators is and will continue to be a limit factor to future progress if no other means of acceleration is developed.

Several novel accelerators techniques currently exists in various stages of development. The most widespread of these is based on the phenomena of *plasma wakefield acceleration*. An ultra-relativistic particle beam or a high intensity laser pulses driven through a pre-formed plasma can excite plasma waves with phase velocities equal to the group velocity of the particle or laser driver [4]. These waves, or 'wakefields', are large-amplitude oscillations of the plasma-electron density which are able to support accelerating electric fields of hundreds of GV/m; thousands of times higher than conventional RF cavities. By injecting an electron, or positron, bunch behind the driver one can then achieve constant acceleration by effectively letting the particle bunch surf the plasma-electron wave. In this manner, provided a sufficiently powerful driver is available, sizeable energy gains can be achieved over relatively short propagation distances. In fact, this form of plasma acceleration was proposed in 1979 by Tajima and Dawson [5], not only as a viable terrestrial particle accelerator but also as a generation mechanism for ultra-high-energy cosmic rays in the plasma rich environment around newly formed pulsars. At the time of their proposal, however, the lack of sufficiently high intensity lasers was a limit factor in exploring these ideas experimentally [6]. The

development of the chirped-pulse laser amplification techniques in 1985 by Strickland and Mourou [7] gave researchers access to ultrashort high-intensity laser pulses. This opened up the possibility of laser-driven plasma wakefield acceleration (LWFA) and several experiments constructed in the following decade were able to successfully demonstrate LWFA of electrons [8]. Recent experiments, propelled by the rapid development of modern multi-terawatt laser facilities, have demonstrated acceleration of electron bunches in a few centimetres of plasma up to 1, 2 and 4 GeV with relatively small energy spreads [9, 10, 11], making LWFA a serious contender for the construction of compact x-ray free-electron lasers [12]. Progress towards even higher energy gains have been made in the last two decades by the construction of dedicated beam-driven plasma wakefield acceleration (PWFA) facilities. Notably, experiments at the Facility for Advanced Accelerator Experimental Tests (FACET) at Stanford aims to use 20 GeV electron and positron beams to drive wakefields which in turn will accelerate secondary electron or positron bunches to higher energies [13]. Furthermore, the Advanced Proton Driven Plasma Wakefield Acceleration Experiment (AWAKE) recently demonstrated proof-of-principle acceleration of secondary electron bunches up to 2 GeV within plasma wakefields driven by the 400 GeV proton beam from CERN’s Super Proton Synchrotron [14]. These experiments are paving the way towards compact high-energy particle accelerators at GeV energies with great promise to science and industry. One can also imagine a future in which plasma wakefield accelerators are used in high-energy physics, perhaps in conjugation with conventional accelerators as a pre-accelerator or energy booster. Even though the latter is probably decades away, both GeV and TeV accelerators might still be able to benefit from plasma wakefield phenomena. Regardless of the means of acceleration, be it larger conventional accelerators or smaller plasma wakefield accelerators, the ultra-relativistic beams produced will need to be dealt with. The current approach for both small and large accelerators is to dump the energy of the beam.

1.2 Beam dumps

When in operation, the energy of the 105 GeV electron and positron beams at the LEP at CERN were dumped by directing them into a 2 m long, 40 cm in diameter, aluminium alloy block [15]. The proposed water-based beam dump for the ILC [16], which is to operate at 500 GeV, is significantly different to its lower energy predecessor at LEP. The increased energy and intensity of the ILC beam makes the extraction of its energy from a solid material beam dumps exceedingly difficult due to the limitations imposed by thermal conduction [16]. By using a tank of water the ILC beam energy can be deposited and removed using a pumping system. However, the high intensity beams will lead to water temperatures in excess of 155°C as well as decomposition of water into hydrogen and oxygen gas. This necessitates a high-pressure vessel and a safe way to remove and store these volatile gases. Furthermore, the beam interaction with the water molecules will create the radioactive nuclei ^3H and ^7Be , which demands a waste-water storage tank. The tank itself will also suffer radiation damages, specifically the window through which the beam enters the vessel. A report by Satyamurthy et al. [16] estimates that this window will need to be replaced at periodic intervals and due to the induced radioactivity this will have to be done remotely using robotic technology. Although this technology is widely available in the nuclear industry this whole beam dump is a large and costly affair for the ILC and any future HEP accelerators. Moreover, not only HEP accelerators face this issue, even metallic or concrete beam dumps for MeV to low GeV accelerators lead to radioactivation which must be carefully assessed and adequately shielded for [17, 18].

An alternative approach aims to utilize the unprecedented acceleration gradients from PWFA. This idea, called a passive plasma beam dump, was proposed in 2010 by Wu et al. [19]. They simulated a 500 MeV electron bunch and showed that an energy loss of up to 70% was achievable by propagating 2 mm through a dense plasma, as shown in figure 1.1. Full energy depletion

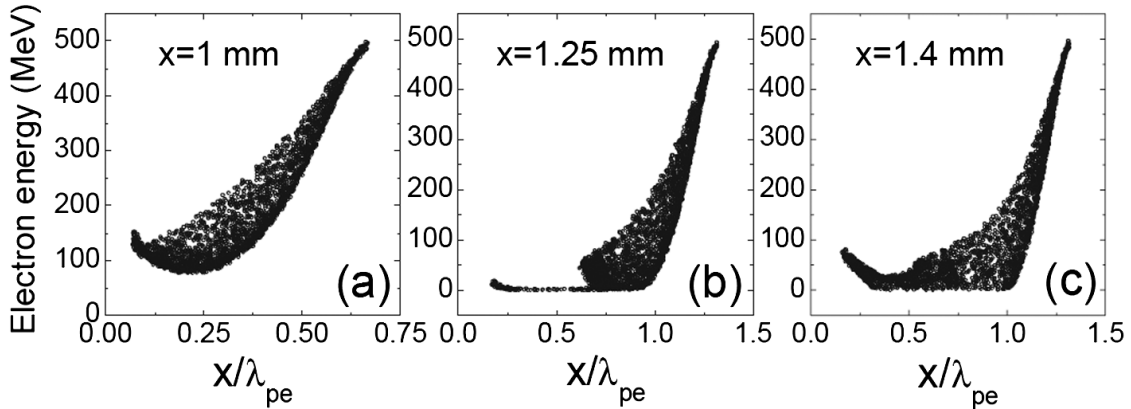


Figure 1.1: Energy distributions of an electron bunch during propagation through a dense plasma, as found by Wu et. al [19]. 1(b) shows non-relativistic particles falling behind the head of the bunch and 1(c) shows their subsequently re-acceleration. The x-axis shows the distance along the bunch in relation to the plasma wavelength, which is covered in chapter 3.

was prevented due to decelerated, non-relativistic, electrons falling behind the head of the bunch, figure 1(b), drifting into an accelerating region the wakefield and subsequently re-accelerated to relativistic energies, figure 1(c). This process prevents further significant energy loss and the deceleration is said to have saturated. It was further demonstrated that the decelerating field is independent of the initial bunch energy by demonstrating that a 100 GeV bunch would require 20 cm to loose 70% of its energy [19]. To minimize re-acceleration the simulated plasma was intersected by aerogel foils, strategically placed to capture the non-relativistic particles. This resulted in an energy loss of 90% for the 500 MeV bunch. It is however not clear how prolonged exposure to plasma and interactions with high-energy electron bunches would affect the degradation of these foils. As an alternative, Hanahoe et al. [20] proposed the use of varying plasma density instead of foils. Linear or quadratically increasing plasma densities were shown to achieve comparable reduction of the re-accelerated particles as the foils used by Wu et al. It is however unclear whether such plasma density profiles can be set up and maintained in a plasma cell. Furthermore, the head of the bunch still maintained its energy in both these approaches; this *energy chirp* is evident in figure 1(c) and occurs because the head of the bunch sets up the wakefield but does not experience the decelerating field itself [19]. For the 500 MeV bunch this might not be a major issue since smaller conventional beam dumps could be used to dump this remaining energy. For GeV energies however this energy chirp may still pose an issue due to radioactivation. To address the energy chirp Bonatto et. al [21] proposed the *active beam dump*, whereby a laser pulse is driven ahead of the bunch through a plasma such that a decelerated wakefield is set up around the bunch. By carefully positioning the laser in relation to a 1 GeV bunch it was shown that the energy in the head of the bunch could be significantly reduced, resulting in total energy losses up to 95%. It is however difficult to extend this method to higher energies due to the dispersion of the laser in the plasma, which prevents laser propagation over the longer distances required.

Given that the active approach is able to reduce the energy chirp and that the passive beam dump leaves behind a pronounced energy chirp, the natural continuation of the previous work is to combine these methods. This project endeavours to demonstrate, through simulations, the successful combination of these methods in what we call a *hybrid beam dump*. This scheme is outlined in figure 1.2. The general approach is to use a passive beam dump to decelerate the bunch until saturation and then pass only the head of the bunch through an active beam dump, instead of decelerating the full-energy bunch with a laser driver as in the work by Bonatto et al.. This should have the added benefit of requiring a less powerful laser as well as being applicable to higher

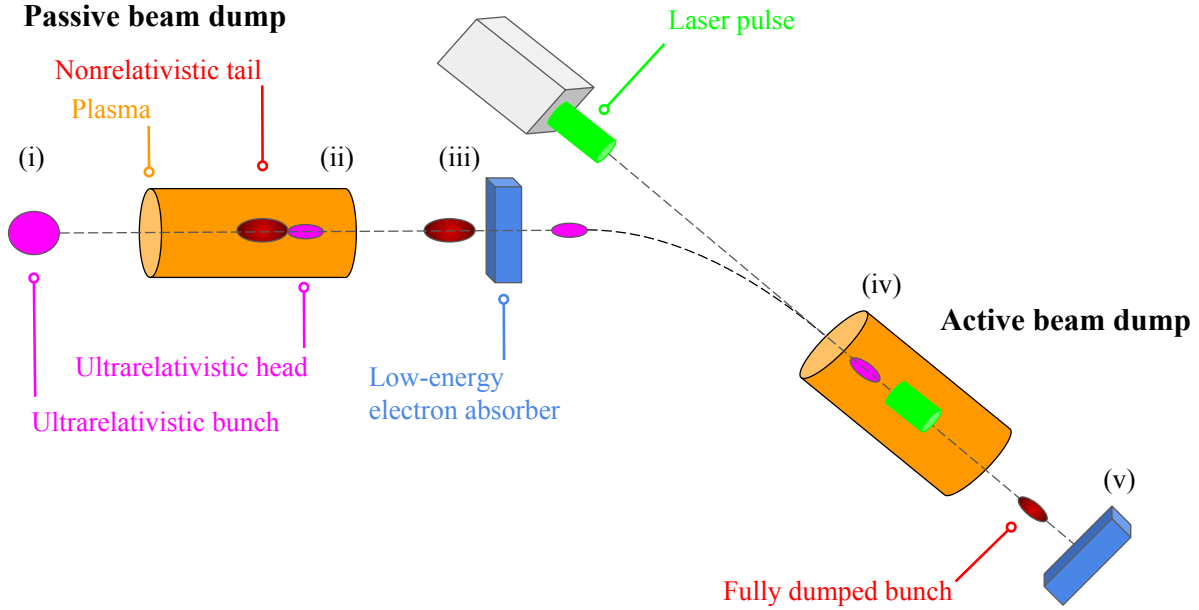


Figure 1.2: Outline of the hybrid beam dump scheme at five stages. (i) The incoming ultra-relativistic (violet) electron bunch passes through vacuum towards the first plasma cell. (ii) The electron bunch loses energy as it propagates through the plasma. A non-relativistic (red) tail of particles is formed behind the the head of the bunch, which maintains its energy. (iii) The non-relativistic tail is removed by propagating through an absorbing material and the path of the head is bent by magnets so as to be aligned behind a laser pulse. (iv) The laser pulse drives a plasma wakefield in front of the remaining bunch, decelerating it to non-relativistic energies. (v) The remaining energy is absorbed.

energies since previous work has shown that the energy chirp contains only $\sim 10\%$ of the initial energy.

1.3 Outline of report

This intermediate report details the initial phase of a full-year project on plasma wakefield deceleration and is written in partial fulfilment of the requirements for the degree of Master in Physics. As such, it does not attempt to cover the full scope of the work and research conducted in this project so far, but rather aims to provide an introduction to the field, establish the theoretical background and construct the computational framework necessary to perform the intended research. Having laid the groundwork for the project in this report, the final-year report will reap the rewards of this work by presenting the full results and outcome of the project.

Chapter 2 of this report details the simulation framework used in this project and chapter 3 covers the theory behind beam-driven plasma wakefields. The theory describing laser-driven plasma wakefields, necessary to understand the active beam dump approach, will be covered in a subsequent report. Simulation tests and preliminary results are presented in chapter 4. We conclude this report by summarising the work that has been presented and looking ahead at the work that is to be carried out in the second half of this project.

2

Simulations

2.1 Plasma simulations

Why simulations

Simulations because: Cheaper than experiments, more readily available to anyone, simulations allow us to study, understand and exploit these phenomena without the need to repeatedly perform expensive and intricate experiments...Furthermore, by having a simulated rather than physical experiment, one may avoid the uncertainties and noise present in the real world and may therefore investigate and even discover physical phenomena that are too sensitive to be detected in noisy data samples. To take advantage of simulations it is however crucial to know the accuracy by which the simulations model the physical situation and to understand the limitations that this imposes. For instance, as will be shown in section XXX, failing to model the experiment with high enough resolution can lead to phenomena emerging from purely numerical features in the simulations. One must therefore be confident that the results seen in simulations accurately represent the physics at hand, either by comparing the simulations to experimental data or theoretical calculations if available. The non-linear nature of the high-energy plasma wakefield phenomena that we wish to model in this project do not lend themselves easily to analytical treatments. To investigate these phenomena and provide useful results for future experiments we will make extensive use of simulations in this project.

Given that a plasma is no more than electrons and ions interacting electromagnetically, the response of such a plasma to the propagation of an electron bunch or laser pulse could in theory be simulated by solving Maxwell's equations for a set of initial conditions. This approach is however computationally intractable due to vast number, $> 10^{15}$, of particles present in the simulations we need to perform. To circumvent this computational road block we make use of so-called Particle-In-Cell (PIC) codes, in which a large collections of physical microscopic particles are represented as smaller collections of macroscopic pseudo-particles on a grid. In this chapter we outline the general PIC approach and introduce the plasma physics PIC code EPOCH, which is used throughout this project. We further detail the modifications necessary to allow the hybrid beam dump scheme to be simulated on EPOCH.

2.2 EPOCH

The Extensible PIC Open Collaboration project (EPOCH) is an advance relativistic electromagnetic PIC code developed at the University of Warwick by XXX et al. [ref.user-manual]. EPOCH is now maintained and developed through the Collaborative Computational Project in Plasma Physics (CCP-Plasma), from which access to the code is granted to non-profit research laboratories and Universities [CCP website]. The underlying code is written in Fortran and allows for simulations to be run on multiple parallel processors via MPI; this enables time-consuming simulations to be run on remote computing clusters. The core PIC code in EPOCH is based upon the field update and particle push algorithms of the Plasma Simulation Code (PSC) written by H. Ruhl []. This

follows closely the standard PIC method outline in section 2.3. The main difference being in how the FTDT method is implemented and the inclusion of additional functionality to allow for more advanced features such as collisions, ionisation and quantum electrodynamic radiation to be simulated [epoch manual].

EPOCH is highly user-friendly; setting up simulations simply requires users to specify the parameters and initial conditions of the simulations without the need to interact with the underlying PIC code. Likewise, analysing and visualising data from a simulations is made easier through file-compatibility with Python, Matlab, IDL and VisIt, the details of which will be covered in this section.

2.3 Particle-in-Cell Codes

Particles are not on yee grid but fields are on yee grid. So rho and J need to be put on yee grid to find fields, and to find new particle positions the fields need to be calculated off-yee grid. However, since the electric field is sourced in part by magnetic flux variations, the fields are solved at intermediate steps.

Since the fields are determined by the position and velocity of the particles, which in turn are determined by the fields, these can not be calculated simultaneously. In its simplest form, PIC codes decouple these calculations by dividing each iterations step into four separate parts. EM fields are fixed on grid, particles move freely Starting from EM fields $\mathbf{E}_{(n)}$, $\mathbf{B}_{(n)}$ and charge current $\mathbf{J}_{(n)}$ present at iteration n [at a specific position, middle of Yee grid?] we obtained the fields at the next time step $n + 1$ by computing the resulting fields and currents at an intermediate half-way step $n + 1/2$. We do this by first computing the change in the electric field, using Ampere's law, $\Delta\mathbf{E}_{(n)}$ which we add to our current field such that

$$\mathbf{E}_{(n+1/2)} = \mathbf{E}_{(n)} + \frac{\Delta t}{2} \left(c^2 \nabla \times \mathbf{B}_{(n)} - \frac{\mathbf{J}_{(n)}}{\epsilon_0} \right) \quad (2.1)$$

from this the magnetic field is given by

$$\mathbf{B}_{(n+1/2)} = \mathbf{B}_{(n)} - \frac{\Delta t}{2} \left(c^2 \nabla \times \mathbf{E}_{(n+1/2)} \right) \quad (2.2)$$

(at which point the particle pusher, detailed below, updates the current to $\mathbf{J}_{(n+1)}$)
at which point we need to update the current to $\mathbf{J}_{(n+1)}$ in order to proceed finding the fields at time step $n + 1$. This is done using the particle pusher. We update the position of each particle

$$\mathbf{x}_{(n+1/2)} = \mathbf{x}_{(n)} + \frac{\Delta t}{2} \mathbf{v}_{(n)} \quad (2.3)$$

from which we also obtain the intermediate velocity $\mathbf{v}_{(n)}$ [correct?]. Using the Lorentz force law we then compute the force $\mathbf{F}_{(n)} = \Delta p / \Delta t$ which gives the momentum at $n + 1$ as

$$\mathbf{p}_{(n+1)} = \mathbf{p}_{(n)} + q \Delta t \left[\mathbf{E}_{(n+1/2)} (\mathbf{x}_{(n+1/2)}) + \mathbf{x}_{(n+1/2)} \times \mathbf{B}_{(n+1/2)} (\mathbf{x}_{(n+1/2)}) \right] \quad (2.4)$$

where, the electric fields are extrapolated (?) to the intermediate point $n + 1/2$. Then, using $\mathbf{p} = \gamma m \mathbf{v}$, we can find the velocity at $n + 1$, from which we then have the current $\mathbf{J}_{(n+1)}$. We then reverse the order of computing such that the magnetic field is calculated prior to the electric field,

$$\mathbf{B}_{(n+1)} = \mathbf{B}_{(n+1/2)} - \frac{\Delta t}{2} \left(c^2 \nabla \times \mathbf{E}_{(n+1/2)} \right) \quad (2.5)$$

$$\mathbf{E}_{(n+1)} = \mathbf{E}_{(n+1/2)} + \frac{\Delta t}{2} \left(c^2 \nabla \times \mathbf{B}_{(n+1)} - \frac{\mathbf{J}_{(n+1)}}{\epsilon_0} \right) \quad (2.6)$$

Using these fields when then calculate the new particles positions $\mathbf{x}_{(n)}$, we "push" the particles, thus completing the iteration step.

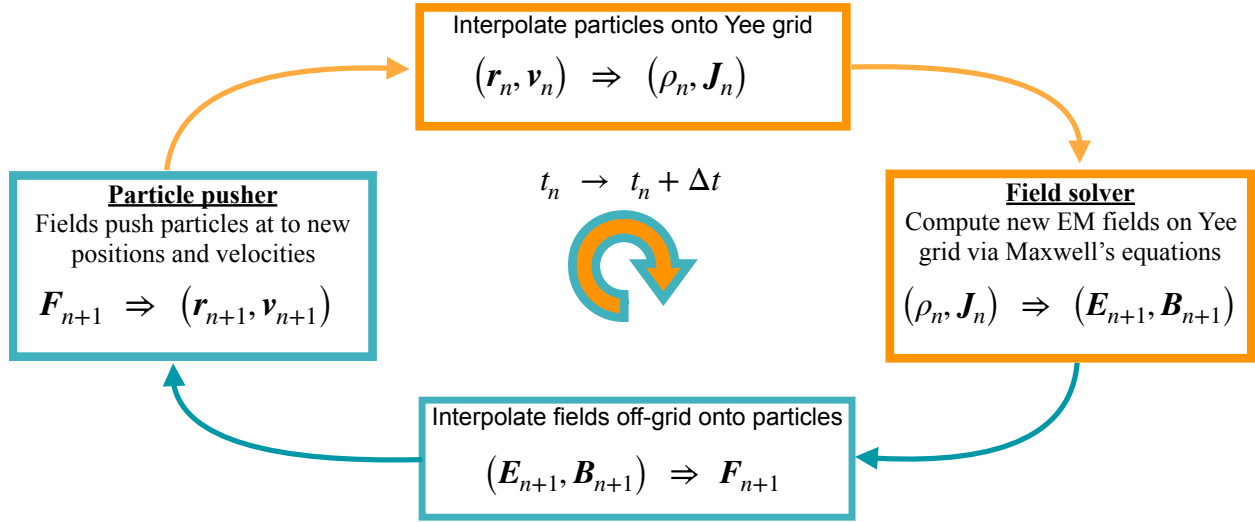


Figure 2.1: The field update and particle push algorithm run b

2.3.1 Input deck

Once EPOCH has been downloaded and compiled the so-called input deck is essentially EPOCH's user interface. This is a file in which users specify the details of a simulations and it is this file that gets read by EPOCH and passed onto the core PIC algorithm. The input deck consists of blocks which define parameters for different features of the simulation.

Explain control block first, and what the restart does. This specifies the grid that the simulations is to run on. We then populate this grid with plasma particles. **Species block,** with explanation about analytical density distributions for plasma, and specify ppc.

The control and species blocks together define the resolution of the simulation. When setting up the resolution of the grid one has to make sure that the grid is sufficiently fine such that the smallest features of our physical system are resolved. This is to ensure that the simulation accurately models the physical system it is meant to represent, to the extent that missing small scale phenomena might alter the large scale outcome of the simulation. A finer grid however requires more macroparticles to fully populate the grid, which inevitably extends the computational time. In addition the time step Δt needs to be suitably decreased as well. This is because of the so-called Courant-Friedrichs-Lowy (CFL) condition. Any simulation introduces uncertainties in the final outcome due to the finite resolution. We need to make sure that the uncertainties introduced during each iteration do not build up and grow unbounded.

2.3.2 Non-analytical bunch initialisation

The hybrid scheme approach that the endeavour to investigate in this project relies on us being able to simulate a laser pulse propagating in front of a pre-saturated bunch. Previous investigations by our colleagues have shown that this is not a trivial task using the simulation software that have been tried. The issue with epoch in this regard is that everything that is to be included in the simulation need to be specified in the input deck and introduced at the begining of a simulation.

Hence, simulations of the active beam dump are entirely possible in EPOCH, since a laser can be initialised in front of a bunch at $t = 0$ and driven together. Introducing a laser at a later stage $t > 0$ appeared however not to be possible. The majority of the work so far in this project has been concerned with solving this issue. The approach taken was to simulate the passive part first and then export the data of the saturated bunch into a new simulation which includes a laser driver. The structure of the SDF data files output by EPOCH are however not suitable for accessing and retrieving particular sets of data. A workaround was found by using VisIt to read the files and subsequently export only the data related to the electron beam. This data was subsequently read by EPOCH during the compilation stage in a specific file included in EPOCH. This file, usually left empty, allows users to over-ride section of the input file by assigning custom values to each of the macroparticles that are initialised in at the start of a simulation. Through this approach we are now able to define a simulation where a laser pulse is driven ahead of a standard bi-gaussian electron beam. By then over-riding the parameters for the electron beam we can then use the data from a pre-saturated bunch to reposition each macroparticle in the bi-gaussian to its corresponding position relative to the rest of the bunch. By also over-riding momentum parameters we can completely mould the bunch into the one we had exported after a passive beam dump.

Real accelerators operate at a range of beam parameters tailored to specific research purposes. In order to avoid having to set up week-long simulations for each minor change of parameters it is crucial to understand the theory underlying these plasma wakefield phenomena and to see to what extent the theoretical predictions match the simulations

For any practical implementation of the hybrid scheme to an existing experiment it

3

Theoretical foundations

3.1 Introduction

In this chapter we introduce the linear fluid model of plasma wakefield acceleration and derive the equations governing the response of a plasma to an electron bunch propagating through. This model assumes that the bunch is ultra-relativistic and that the plasma density is much higher than the bunch density, which will allow us to treat the plasma response as a first order perturbation to the background density. We also discuss the non-linear, so-called "blowout", regime which can not be treated perturbatively and is characterised by the expulsion of plasma electrons in a volume behind the bunch. The response to a laser being driven through the plasma, the so-called ponderomotive force response, shares many similar features to the theory presented in this chapter but presents other issues such as dissipation and de-phasing in the plasma which will need to be addressed in the context of the active beam dump. For this reason the theory of laser-plasma interactions will be covered in a subsequent report.

3.2 Linear fluid model

In this section, we derive the response of a plasma to an electron bunch by considering the plasma electrons as a fluid. We shall make the assumptions; (i) the initial plasma is uniform and electrically neutral everywhere; (ii) the plasma ions can be considered stationary since for all plasmas the mass of the ions is much larger than the electron mass, $m_{\text{ion}} \gg m_e$; (iii) the electron bunch is ultra-relativistic, $v/c \approx 1$, such that the density distribution of the bunch does not evolve as it interacts with the plasma; (iv) the bunch density is much less than the plasma electron density, $n_b \ll n_p$. A beam propagating through a plasma satisfying these conditions is said to be in the *linear regime*. The dynamics of the plasma electrons is governed by the continuity equation

$$\frac{\partial n_p}{\partial t} = -\nabla \cdot (n_p \mathbf{v}_p) \quad (3.1)$$

where n_p is the plasma electron density density and \mathbf{v}_p the plasma fluid velocity. This simply ensures charge conservation by imposing that the plasma electron density change in a given volume is due to plasma electrons flowing in or out. The evolution of the electromagnetic fields in the plasma is governed by Maxwell's laws:

$$\nabla \cdot \mathbf{E} = 4\pi\rho \quad (3.2)$$

$$\nabla \cdot \mathbf{B} = 0 \quad (3.3)$$

$$\nabla \times \mathbf{E} = -\frac{1}{c} \frac{\partial \mathbf{B}}{\partial t} \quad (3.4)$$

$$\nabla \times \mathbf{B} = \frac{4\pi}{c} \mathbf{J} + \frac{1}{c} \frac{\partial \mathbf{B}}{\partial t} \quad (3.5)$$

which in turn determine the response of the plasma fluid through the Lorentz force law:

$$m_e \frac{\partial n_p \mathbf{v}_p}{\partial t} = e n_p \left(\mathbf{E} + \frac{\mathbf{v}_p \times \mathbf{B}}{c} \right). \quad (3.6)$$

We now make use of assumption (iv) which allows us to treat the plasma response to a particle beam perturbatively such that $n_p = n_0 + n_1$, where n_0 is the unperturbed uniform electron density and $n_1 \ll n_0$ is the perturbation from interacting with the electron bunch. This perturbation also requires that the change in fluid velocity upon interacting with the bunch is small, such that $v_p \ll c$. Substitution into the continuity equation yields

$$\frac{\partial n_1}{\partial t} = -n_0 \left(1 - \frac{n_1}{n_0} \right) \nabla \cdot \mathbf{v}_p \quad (3.7)$$

Taking the time differential and neglecting terms $\mathcal{O}(n_1/n_0)$ then gives

$$\frac{\partial^2 n_1}{\partial t^2} = -n_0 \frac{\partial(\nabla \cdot \mathbf{v})}{\partial t} \quad (3.8)$$

Similarly, substitution into the Lorentz force law gives to first-order

$$m_e \frac{\partial \mathbf{v}}{\partial t} = e \mathbf{E} \quad (3.9)$$

which, using Gauss's law, gives

$$\frac{\partial(\nabla \cdot \mathbf{v})}{\partial t} = \frac{e^2}{m_e} 4\pi(n_1 + n_b) \quad (3.10)$$

where n_b is the charge density of the electron bunch. Equations (3.8) and (3.10) hence give

$$\frac{\partial^2 n_1}{\partial t^2} + \omega_p^2 n_1 = -\omega_p^2 n_b \quad (3.11)$$

where

$$\omega_p = \sqrt{\frac{4\pi e^2 n_0}{m_e}} \quad (3.12)$$

is the plasma frequency. Hence the plasma density perturbation is described by a second-order differential equation with the bunch acting as a source term. We proceed to solve this for a radially symmetric bunch by evaluating equation (3.11) in a reference frame co-moving with the electron bunch [22], where the coordinate $\xi = x - ct$ represents the position along the bunch as it travels in the x -direction. Doing this yields

$$-\frac{1}{k_p^2} \left(\frac{\partial^2}{\partial \xi^2} + k_p^2 \right) n_1(r, \xi) = n_b(r, \xi) \quad (3.13)$$

where $k_p = \omega_p/c$ is the wavenumber and causality demands that $n_1(r, \xi < 0) = 0$. We evaluate this by finding the Green's function $G(\xi, \xi')$, which by definition obeys

$$-\frac{1}{k_p^2} \left(\frac{\partial^2}{\partial \xi^2} + k_p^2 \right) G(\xi, \xi') = \delta(\xi - \xi') \quad (3.14)$$

which gives

$$G(\xi, \xi') = \begin{cases} 0 & , -\infty < \xi < \xi' \\ A(\xi') \sin(k_p \xi) + B(\xi') \cos(k_p \xi) & , \xi' < \xi < \infty \end{cases} \quad (3.15)$$

where the constant $A(\xi')$ and $B(\xi')$ are determined by requiring continuity at $\xi = \xi'$ and by integrating equation (3.14) across this same boundary. This yields

$$G(\xi, \xi') = k_p \Theta(\xi - \xi') (\cos(k_p \xi) \sin(k_p \xi') - \cos(k_p \xi') \sin(k_p \xi)) \quad (3.16)$$

and the resulting plasma perturbation is

$$\begin{aligned} n_1(r, \xi) &= \int_{-\infty}^{\infty} G(\xi, \xi') n_b(r, \xi') d\xi' \\ &= \int_{-\infty}^{\xi} \sin(k_p(\xi - \xi')) n_b(r, \xi') d\xi' \end{aligned} \quad (3.17)$$

where we have used the trigonometric identity for $\sin(k_p(\xi - \xi'))$. Hence the electron bunch induces oscillatory density perturbations in the plasma with a wavelength given by $\lambda_p = 2\pi/k_p$. In addition, the magnitude of these perturbation scales linearly with n_b , the density of the beam driver. Equation (3.12) further shows that these perturbations scale as $n_0^{(1/2)}$, the square root of the plasma density. These perturbations set up electromagnetic fields in the plasma behind the beam driver. An understanding of these fields is crucial in order to design a functioning plasma wakefield experiment.

3.2.1 Longitudinal Accelerating Field

The electric field parallel to the propagation of the beam driver is what drives particles to either accelerate or decelerate. This is called the longitudinal plasma wakefield and in this section we proceed to derive an expression for it in the linear regime considered above. From Maxwell's equations (3.2-3.5) it is straightforward to show that the electric field in the plasma obeys a wave equation:

$$\nabla^2 \mathbf{E} - \frac{1}{c^2} \frac{\partial^2 \mathbf{E}}{\partial t^2} = \frac{4\pi}{c^2} \frac{\partial \mathbf{J}}{\partial t} + 4\pi \boldsymbol{\nabla} \rho \quad (3.18)$$

where the change in current and variations in the charge density act as source terms. Letting $\rho = \rho_b + \rho_p$ be the total charge density and $\mathbf{J} = \mathbf{J}_b + \mathbf{J}_p$ be the total charge current, where b and p denote the beam and plasma respectively, we have from equation (3.9) that

$$\frac{\partial \mathbf{J}_p}{\partial t} = \frac{e^2 n}{m} \mathbf{E} \quad (3.19)$$

Substituting this into equation (??), together with $\mathbf{J}_b = c\rho_b \hat{\mathbf{z}}$, and taking the z-component gives

$$\left(\nabla^2 - \frac{1}{c^2} \frac{\partial^2}{\partial t^2} - k_p^2 \right) E_z = \frac{4\pi}{c} \frac{\partial \rho_b}{\partial t} + 4\pi \frac{\partial}{\partial z} (\rho_b + \rho_p) \quad (3.20)$$

where $k_p = \omega_p/c$ is the plasma wave number and E_z is the longitudinal electrical field. To solve this we write $\nabla^2 = \nabla_\perp^2 + \partial_z^2$ in transverse and longitudinal components. Furthermore, we proceed to work in Fourier transform space, where

$$E_z(\xi) = \frac{1}{2\pi} \int_{-\infty}^{\infty} \tilde{E}_z(k) e^{ik\xi} dk \quad (3.21)$$

and similarly for ρ_b and ρ_p . Equation (3.20) now simplifies to

$$\left(\nabla_\perp^2 - k_p^2 \right) \tilde{E}_z(\xi) = 4\pi i k \tilde{\rho}_p, \quad (3.22)$$

We note that the two contributions from the beam, \mathbf{J}_b and ρ_b , have cancelled each other out. This is because the beam velocity was set to be ultrarelativistic, $\beta = 1$, such that the electric field

witnessed by the stationary plasma electrons is purely in the radial direction [23]. The effect of the beam is however represented in the plasma modulations through equation (3.17). It is convenient to write this relationship in a compact form by taking the Fourier transform of equation (3.11) to find that

$$\tilde{\rho}_p = \frac{k_p^2}{k^2 - k_p^2} \tilde{\rho}_b . \quad (3.23)$$

which together with the cylindrical representation of the Laplacian

$$\nabla_{\perp}^2 = \frac{1}{r} \frac{\partial}{\partial r} r \frac{\partial}{\partial r} + \frac{1}{r^2} \frac{\partial^2}{\partial \phi^2} \quad (3.24)$$

gives

$$\left(\frac{\partial^2}{\partial r^2} + \frac{1}{r} \frac{\partial}{\partial r} - k_p^2 \right) \tilde{E}_z = 4\pi i k_p^2 \frac{k}{k^2 - k_p^2} \tilde{\rho}_b \quad (3.25)$$

where we have assumed that the longitudinal field is radially symmetric. This is the Fourier transformed version of equation (3.20), which has the advantage of the source term being a function of the Fourier transform of the beam density alone. At this point it should be noted that a setting the beam velocity to $\beta = 1$ before solving this equation, as we have done here, is technically not valid..... However, the effect of this is altogether negligible in our case (calc extra term from their paper).

We now rewrite this equation as

$$\mathcal{L} \tilde{E}_z = \tilde{f}(r) \quad (3.26)$$

Hence by solving this PDE we can find E_z through inverse the Fourier transform. We do this by finding its Green's function $G(\mathbf{r}, \mathbf{r}')$. Working in a cylindrical coordinate system we have that the Green's function must satisfy

$$\mathcal{L} G(\mathbf{r}, \mathbf{r}') = \frac{1}{r} \delta(r - r') \delta(\phi - \phi') \delta(z - z') \quad (3.27)$$

where the 3-dimensional Dirac delta function is written in cylindrical polar coordinates and defined such that $\int \delta(\mathbf{r} - \mathbf{r}') r dr d\phi dz = 1$. Since the PDE is a function of the radius we can write the Green's function as

$$G(\mathbf{r}, \mathbf{r}') = G_r(r, r') \delta(\phi - \phi') \delta(z - z') \quad (3.28)$$

which leads to

$$\mathcal{L} G_r(r, r') = \frac{1}{r} \delta(r - r') \quad (3.29)$$

The left-hand side of this expression is the modified Bessel function of order zero [24]. Consequently, the Green's function is formed by linear combinations of the two modified Bessels functions of order zero, which we denote by K_0 and I_0 :

$$G(r, r') = \begin{cases} A(r')(A_1 I_0(k_p r) + B_1 K_0(k_p r)) & , 0 < r < r' \\ B(r')(A_2 I_0(k_p r) + B_2 K_0(k_p r)) & , r' < r < \infty . \end{cases} \quad (3.30)$$

By requiring that the two parts of this expression each satisfy one of the boundary conditions we have that $B_1 = A_2 = 0$ since $K_0(k_p r) \rightarrow \infty$ as $r \rightarrow 0$ and $I_0(k_p r) \rightarrow \infty$ as $r \rightarrow \infty$. Continuity in $G(r, r')$ at $r = r'$ further gives that

$$G(r, r') = A_0 \begin{cases} I_0(k_p r) K_0(k_p r') & , 0 < r < r' \\ I_0(k_p r') K_0(k_p r) & , r' < r < \infty \end{cases} \quad (3.31)$$

where A_0 is a constant of proportionality that we find by integrating equation (3.29) for $r \in [r' - \epsilon, r' + \epsilon]$. This expression needs to be satisfied for all ϵ , including the limit as $\epsilon \rightarrow 0$, such that

$$\lim_{\epsilon \rightarrow 0} \int_{r'-\epsilon}^{r'+\epsilon} \mathcal{L}G_r(r, r') dr = \lim_{\epsilon \rightarrow 0} \int_{r'-\epsilon}^{r'+\epsilon} \frac{1}{r} \delta(r - r') dr \quad (3.32)$$

which gives

$$\left. \frac{A_0}{k_p} \left(I_0(k_p r') \frac{\partial K_0(k_p r)}{\partial r} - \frac{\partial I_0(k_p r)}{\partial r} K_0(k_p r') \right) \right|_{r=r'} = \frac{1}{r'} . \quad (3.33)$$

This equality must hold for all finite values of r' . Hence, following an approach by Jackson [24], we evaluate this expression for $k_p r' \gg 1$, where I_0 and K_0 take the limiting forms:

$$I_0(k_p r') \rightarrow \frac{1}{\sqrt{2\pi k_p r'}} e^{k_p r'} \quad \text{and} \quad K_0(k_p r') \rightarrow \sqrt{\frac{\pi}{2k_p r'}} e^{-k_p r'} \quad (3.34)$$

which implies that $A_0 = -1$. The Green's function can then be written, using the Heavieside step function $\Theta(r)$, as

$$G(r, r') = -I_0(k_p r)K_0(k_p r')\Theta(r' - r) - I_0(k_p r')K_0(k_p r)\Theta(r - r') . \quad (3.35)$$

We can thus find \tilde{E}_z from

$$\tilde{E}_z(r, k) = \int_0^\infty G(r, r') f(r', k) r' dr' \quad (3.36)$$

and then perform an inverse Fourier transform to find

$$E_z(r, \xi) = -2ik_p^2 \int_{-\infty}^{\infty} \frac{ke^{ik\xi}}{k^2 - k_p^2} dk \int_0^\infty (I_0(k_p r)K_0(k_p r')\Theta(r' - r) + I_0(k_p r')K_0(k_p r)\Theta(r - r')) \tilde{\rho}_b(r') r' dr' \quad (3.37)$$

For a known beam distribution $\rho_b(r, \xi)$ this expression can be used to compute the resulting longitudinal electric field. Of particular interest to us is the field induced by the propagation of a bi-Gaussian electron bunch. To compute this we follow an approach by Dawson [25] and first evaluate the field due to a point-particle and then convolve it with our bi-Gaussian driver. We choose a radially symmetric charge distribution ρ_0 with a delta function in the ξ direction so as to match our Green's function:

$$\rho_0(r, \xi) = \frac{e}{2\pi r} \delta(r - r') \delta(\xi) \quad (3.38)$$

Substituting the Fourier transform of this into equation (3.37) and performing a contour integrating in k -space yields

$$E_z(r, \xi) = -2ek_p^2 \cos(k_p \xi) G(r, r') \Theta(\xi) , \quad (3.39)$$

where $\Theta(\xi)$ ensures causality is preserved. This is the so called single-particle wake function [25]. The longitudinal electric field resulting from an arbitrary radially-symmetric source distribution $n_b(r, \xi)$ is now given by convolving the source by the single-particle wake function:

$$E_z(r, \xi) = -2ek_p^2 \int_0^{2\pi} d\phi \int_{-\infty}^{\infty} \cos(k_p(\xi - \xi')) \Theta(\xi - \xi') d\xi' \int_0^\infty G(r, r') n_b(r', \xi') r' dr' \quad (3.40)$$

$$= -4\pi ek_p^2 \int_{-\infty}^{\xi} \cos(k_p(\xi - \xi')) d\xi' \int_0^\infty G(r, r') n_b(r', \xi') r' dr' \quad (3.41)$$

The electric force is thus $F_z(r, \xi) = -eE_z(r, \xi)$. To compare with simulations and experiments we now choose to convert from CGS to SI units by having $e^{\text{CGS}} \rightarrow e^{\text{SI}}/\sqrt{4\pi\epsilon_0}$. The electric force in SI units (J/m) is thus

$$F_z(r, \xi) = \frac{e^2 k_p^2}{\epsilon_0} \int_{-\infty}^{\xi} \cos(k_p(\xi - \xi')) d\xi' \int_0^{\infty} G(r, r') n_b(r', \xi') r' dr' \quad (3.42)$$

To further understand this electric field and its relation to the electron beam we will calculate this numerically for a bi-gaussian bunch with a density of the form

$$\rho_b(r, \xi) = \frac{N_b}{(2\pi)^{3/2} \sigma_r^2 \sigma_\xi} e^{-\xi/(2\sigma_\xi^2) - r/(2\sigma_r^2)} \quad (3.43)$$

where N_b is the number of electrons in the bunch and σ_ξ and σ_r are the standard deviation of the bunch in the longitudinal and transverse direction. We choose the plasma density $n_p = 100n_b$ to ensure that the electron beam is in the linear regime. At this point, to show that the linear fluid model is valid, we also compare this calculation to a simulation of the same situation. The way in which this simulation has been done is covered extensively in chapter 3. The result of this is shown in figure 3.2. We note that the theoretical calculations and the simulations are indeed in good agreement, with the model predicting both the amplitude and the wavelength of the induced electric fields in the plasma. We further note that the electric field is positive along the bunch, which implies that the force on the electron bunch is opposite the direction of travel. Hence the electron bunch in this case should lose energy and slow down. This might at first sight appear unsurprising, since if the bunch moved through a solid material it would lose energy as well, and as the bunch moves through the plasma it displaces electrons which transfers kinetic energy to the plasma. The surprise here however is the uneven way in which the plasma electrons rearrange themselves. Each electron displaces plasma electrons, and each electron transfers a small amount of energy to the plasma electrons, the plasma electrons arrange themselves in such a way as to collectively create a large electric field in the middle of the bunch. So even though each electron transfers some energy kinetically, the ones in the middle will lose a lot more energy through this decelerating electric field which all the electrons in the bunch have contributed to setting up. This is particularly evident for the head of the bunch, which according to both the theory and the simulations should experience a zero value electric field and therefore only lose energy through scattering mechanisms, which is entirely negligible compared to the electric field. Hence, in contrast to propagation through solid matter we expect the head of the bunch to maintain its energy when moving through a plasma. We may furthermore predict that this method can not fully deplete the energy of the beam on its own. For, assuming that the electric field maintains its form as the beam propagates, as soon as particles lose enough energy and fall behind the rest of the bunch, they will end up in a region of positive electric field and subsequently get reaccelerated. One method for dealing with this was described in chapter 1, whereby Wu et al. simulated the use of foils to prevent particles reaching the reacceleration region. The other method, proposed by Hanahoe et al. was to let the beam propagate through an increasing plasma density. Although this method has not been simulated so far, if the proposed experiment at FLASHForward at DESY in 2019 include the possibility to test this proposal this method will need to be explored further in the upcoming report. This method utilizes the transverse wakefields and we cover them below for completeness.

3.2.2 Transverse Field

An ultrarelativistic electron bunch will be highly contracted in the direction of propagation relative to the plasma electrons in the 'lab' frame. Assuming $\beta = 1$ as before the electric field due to the bunch is purely radial, E_r . In addition, the magnetic field due to the charge is azimuthal, B_θ . The

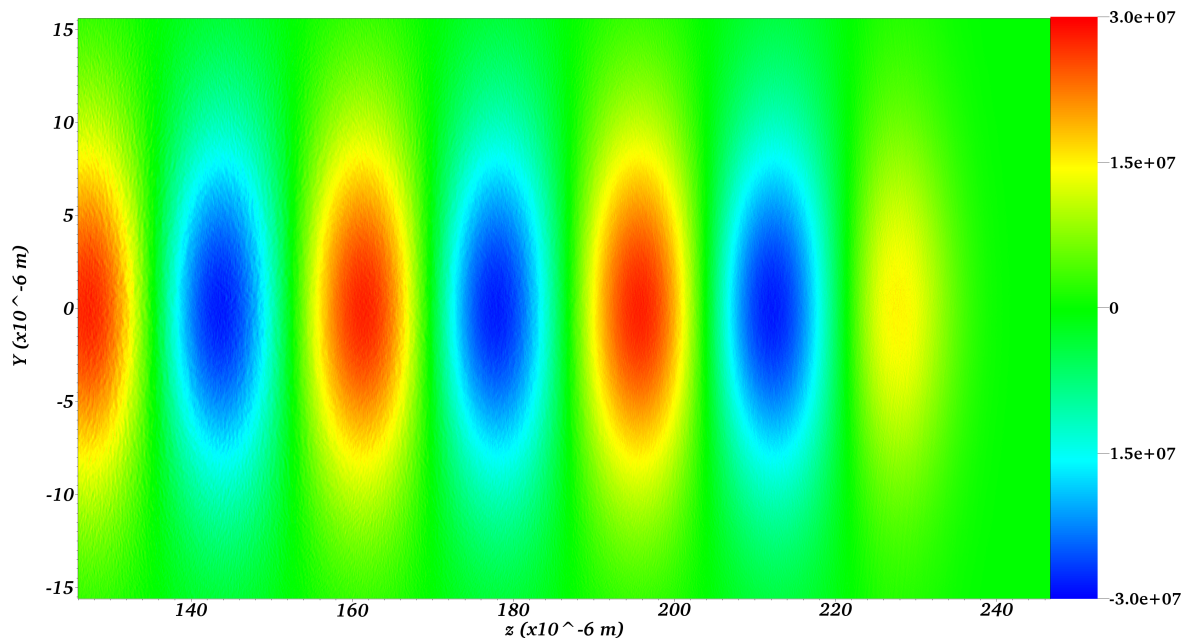


Figure 3.1: •

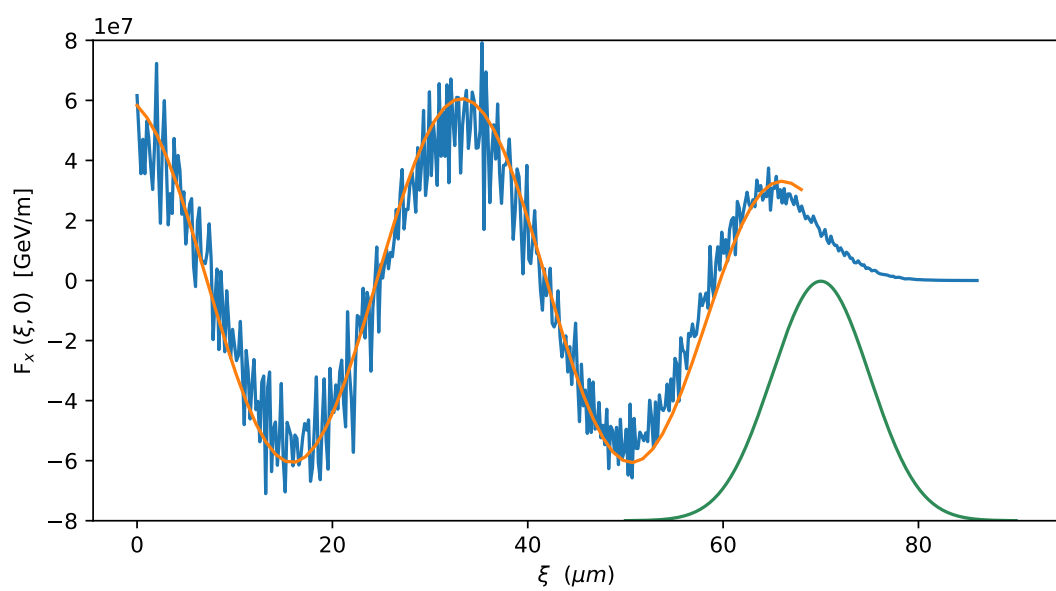


Figure 3.2: Simulation vs. theory for linear regime with $n_p/n_b = 100$.

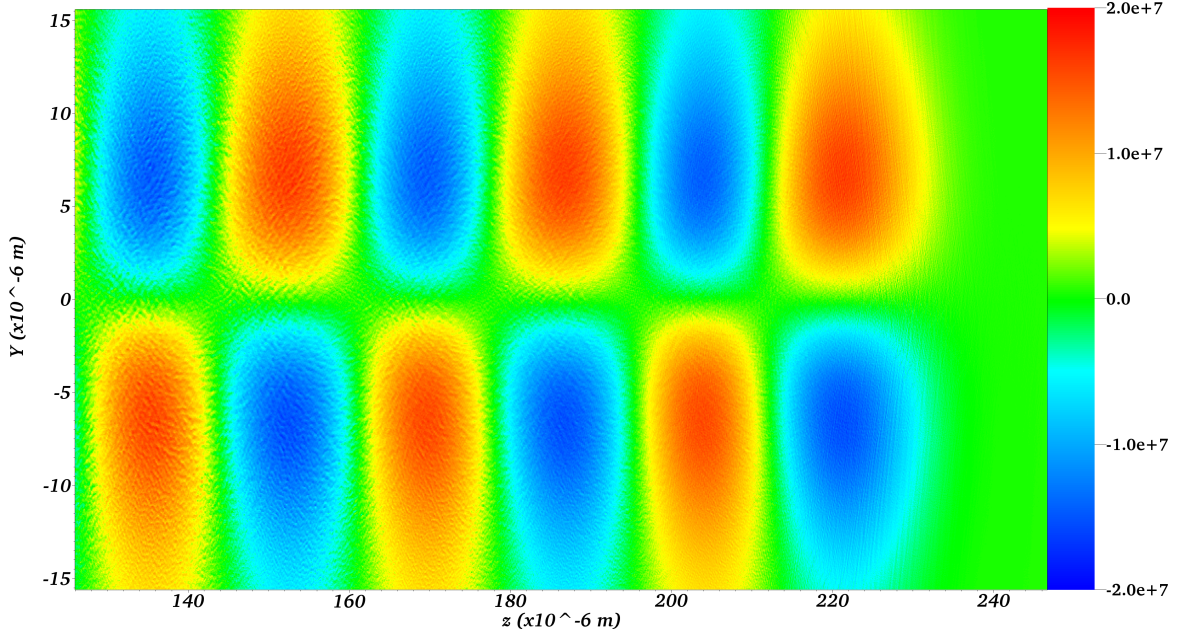


Figure 3.3: •

resulting transverse wakefield $W_{\perp} = E_{\perp} - cB_{\theta}$ experienced by a realtivisit particle due to the wake is given by the *Panofsky-Wenzel theorem*[26], which says that the transverse wakefield at a position $\xi = z - ct$ behind the head of the bunch is related to the longiduinal wakefield W_{\parallel} via

$$\frac{\partial W_{\perp}}{\partial z} = \frac{\partial W_{\parallel}}{\partial r} . \quad (3.44)$$

Since $W_{\parallel} = E_z$ this gives a transverse wakefield

$$W_{\perp}(\xi) = \int \frac{\partial E_z}{\partial r} dz . \quad (3.45)$$

The transverse force on a bi-Gaussian bunch can now by found by applying this expression to on the longitudinal single-particle wakefield (3.39) and then performing the same convolution as above [25, 27], which yields

$$F_r(r, \xi) = -\frac{e^2 k_p}{\epsilon_0} \int_{-\infty}^{\xi} \sin(k_p(\xi - \xi')) d\xi' \int_0^{\infty} \frac{\partial G(r, r')}{\partial r} \frac{\partial n_b(r', \xi')}{\partial r'} r' dr' \quad (3.46)$$

From this we note that the radial field exhibits the same oscillatory behaviour that we have seen before and that the phase of the transverse and longitudinal fields differ by $\pi/2$. This is of particular importance to plasma wakefield acceleration experiments, since it implies that there will be a region which is simultaneously accelerating and focusing, enabling high acceleration of narrow beams. Hanahoe et al. was able to use a similar appraoch to show that by employing a varying density one could find that reacceleration of particles that had fallen behind the bunch occurred in a defocusing region. Thereby forcing the particles outwards, where they were subsequently decelerated through ordinary scattering. Figure ??.

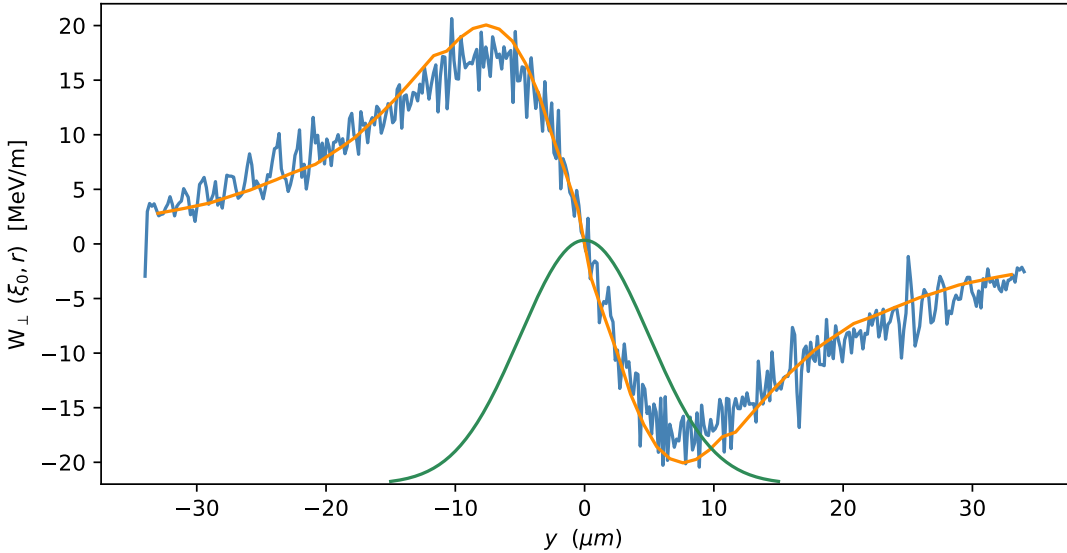


Figure 3.4: Transverse force - theory vs. simulation

3.2.3 Collective Plasma Deceleration – Linear regime

As described above parts of the electron bunch can be in either accelerating or decelerating regions. The parts of the bunch that are in a decelerating region will lose energy; this is the general idea behind a plasma beam dump. Since we can calculate the electric field at any position (ξ, r) along the bunch we can estimate the energy loss by calculating the work carried out by the longitudinal electric field. Since the beam is assumed to be rigid in the linear regime this does not take into account accelerated particles. This is the approach taken by Bonatto et al. to estimate the distance required to dump various beams in passive or active plasma beam dumps [28], and as we shall see in section XXX this approach provides good agreement with simulations.

The rate of energy change with propagation distance of a particle at position (r, ξ) in the bunch after travelling is given by the force exerted on the particle by the longitudinal electric field:

$$\frac{dU_p}{ds} = -eE_z(r, \xi) \quad (3.47)$$

where we have assumed that there occurs no modulation of the particle bunch as it traverses the plasma, hence the electric field is only a function of the position in the bunch $E_z(r, \xi)$ and not the propagation distance s . Integrating over the propagation distance then gives the energy of one particle in the beam at position (r, ξ) after travelling a distance s :

$$U_e(r, \xi, s) = U_e(r, \xi, 0) - seE_z(r, \xi) \quad (3.48)$$

from which multiplication by the beam number density $n_b(r, \xi)$ and integration over the volume of the bunch gives the total energy of all particles in the bunch after propagation distance s

$$U(s) = \int U_e(r, \xi, 0) n_b(r, \xi) r dr d\xi d\phi - se \int E_z(r, \xi) n_b(r, \xi) r dr d\xi d\phi \quad (3.49)$$

where E_z and n_b are found from equations (3.42) and (3.43). A program to compute this numerically has not yet been implemented, but we endeavour to do so in the latter part of this project to allow for comparisons between the linear theory, simulations and hopefully with experimental data from the FLASHForward facility at DESY.

3.3 Non-linear Regime

Lower density, larger plasma response, not possible to describe perturbatively. Hamiltonian approach taken by Lu. et al []

Self-injection?

4

Simulation tests

The initial phase of this project involved simulating beam dumping of the proposed electron beam of the EuPRAXIA project. This is a EU-funded project involving XXX nations and XXX institutions. The ultimate aim is to create a compact 5 GeV laser-driven plasma wakefield accelerator for electrons, combined with an undulator to generate high-quality x-rays for research and medicine. Currently the studies are concerned with generating a high-quality 1 GeV electron beam. As the simulations and experiments yield successful results the energy will be increased until the 5 GeV goal is reached. The electron beam parameters for this beam are given in table 4.1, where case 1 and 2 represents expected electron beam results for laser-driven and beam driven accelerators respectively. In addition, the parameters for our 1 GeV simulations are also shown. These have been chosen so as to represent expected achievable values for both cases [eupraxia2020].

EuPRAXIA bunch parameters			
Parameter	Case 1	Case 2	Simulations
Energy	5 GeV	3 GeV	1 GeV
Charge	100 pC	30pC	30pC
Bunch length (RMS)	1.5 μm	0.9 μm	1.5 μm
Bunch width (RMS)	0.3 μm	0.3 μm	0.3 μm
Energy spread (RMS)	5%	5%	1%
Transverse divergence (RMS)	0.32 mrad	0.41 mrad	10 μrad

Table 4.1: Parameters for the electron bunch in the EuPRAXIA project.

4.1 Plasma deceleration - Uniform density

The EuPRAXIA project endeavours to explore what is achieve in a compact plasma wakefield accelerator with current and expected future technologies. For this reason it is interesting to explore the beam dumping quality that the current plasma technologies can achieve. Working with the simulation beam in table 4.1 we know from equations 3.49 and 3.42 that the shortest beam dumping distance is achieved with the highest possible plasma density, provided that the beam is contained within the decelerating region as shown in figure 3.2. Most plasma wakefield experiments use plasma densities $< 10^{18}\text{cm}^{-3}$ [ref...]. These are achieved using plasma discharge tubes.... These can provide highly uniform plasmas over several meters.

Higher densities, up to $\sim 10^{20}\text{cm}^{-3}$, are however achievable using supersonic gas jets [29]. This technique forces gas through a thin nozzle from a high-pressure region into a vacuum container creating a high-density gas jet. This jet can then be ionised using a laser to generate the desired high-density plasma. Currently these techniques are used to generate plasmas up to a centimetre in length. The result of letting our 1 GeV electron bunch propagate through a plasma of 10^{20}cm^{-3} is shown in figures 1a-c. These show the average energy of particles with respect to their position in the bunch.

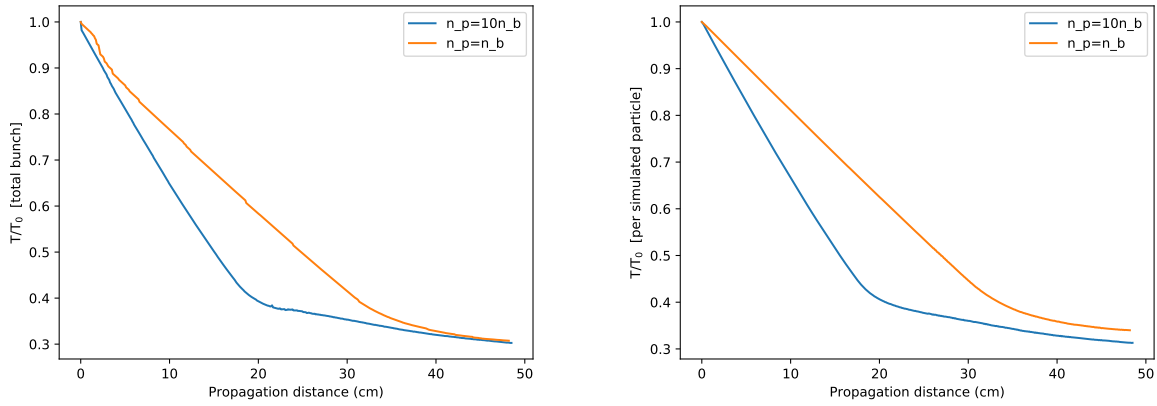


Figure 4.1: •

4.2 Larger bunch

The ideal bunch parameters for the EuPRAXIA beam outlined in table 4.1 lead to bunch densities in excess of 10^{20}cm^{-3} , making neither linear nor quasilinear regimes accessible for beam dumps. An alternative approach is to let the bunch expand, thereby lowering its density, before entering the plasma. Expansion in the radial direction could be achieved by simply letting the bunch propagate freely in a vacuum, which would cause the bunch to expand due to the space-charge force of the electron bunch. Longitudinal stretching could be achieved using a magnetic

We choose here to expand the dimensions of the bunch to $\sigma_z = \sigma_r = 5\text{\mu m}$. This is chosen in part to give a more workable bunch density, 10^{17}cm^{-3} , as well as to allow for comparisons with existing plasma wakefield experiments which tend to have bunch dimensions in the single to tens of micrometer range.

4.2.1 Transverse instabilities in quasilinear regime

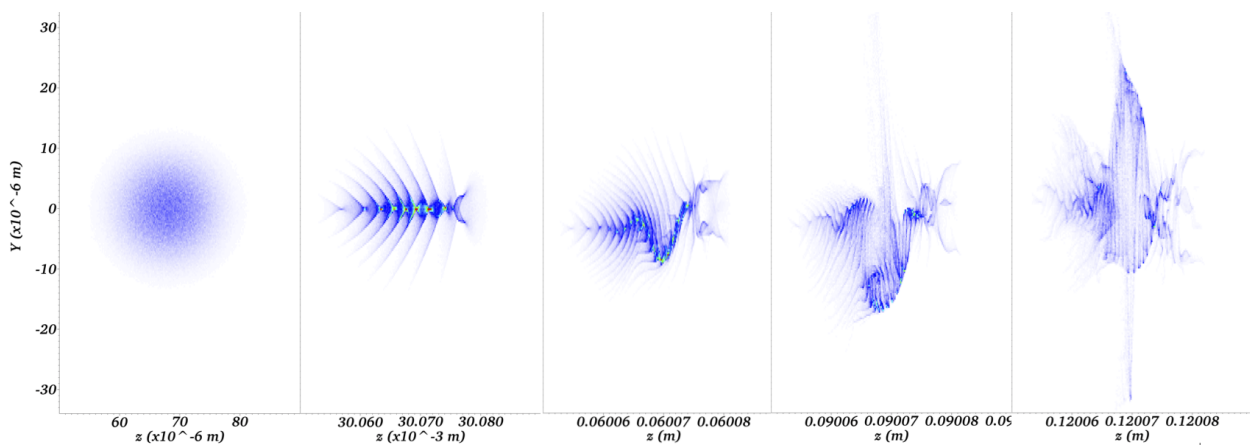
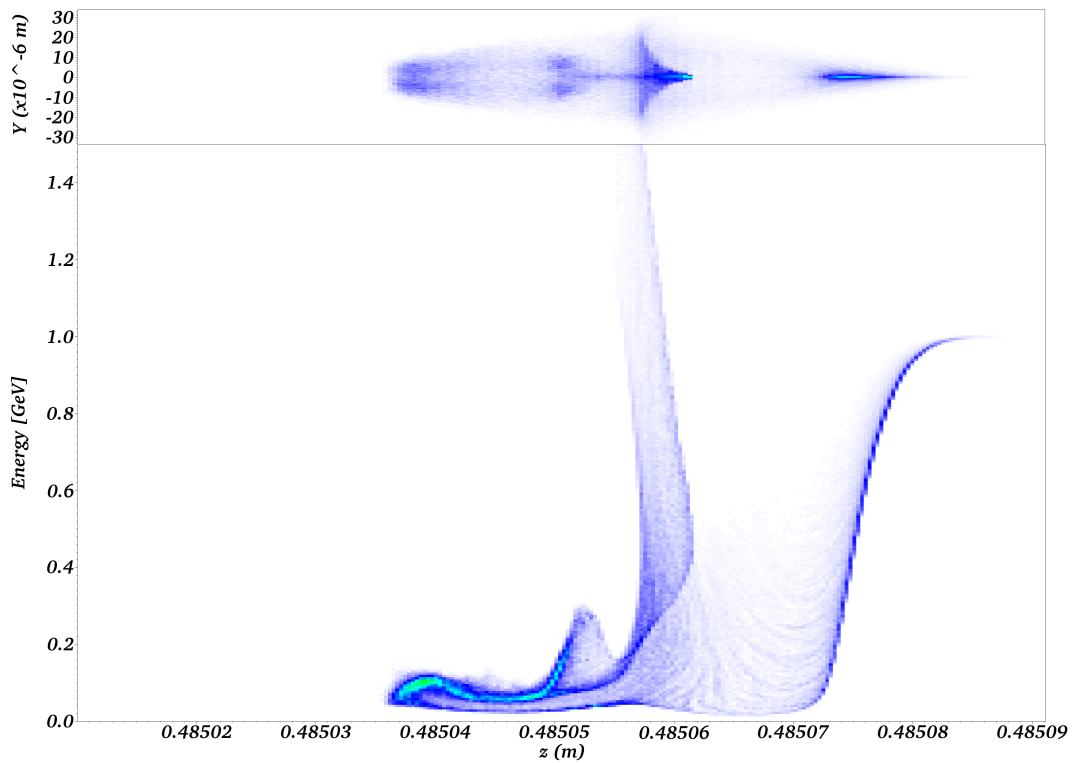
4.3 Hybrid Scheme - Feasibility study

4.3.1 Initialising a decelerated bunch

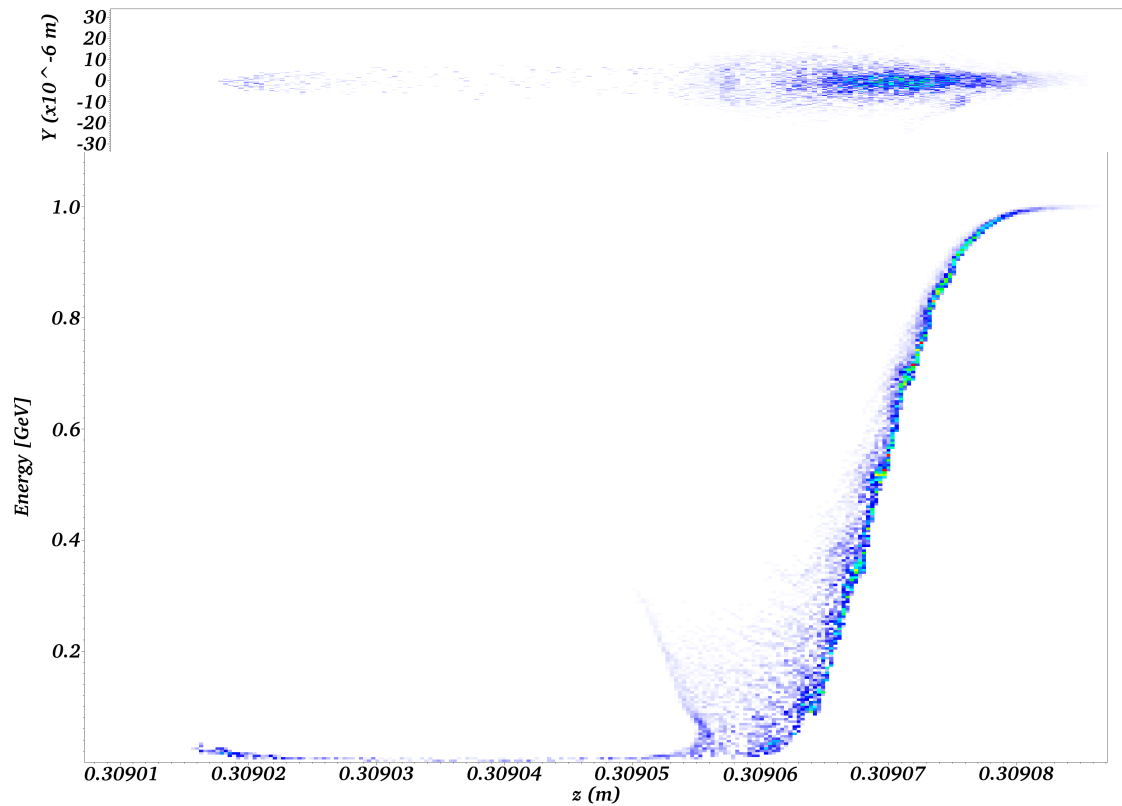
-Compare to actual already propagated bunch we want to simulate. See how quickly the uniform plasma resembles that of the plasma of the propagated simulation. If it takes long time then the laser results might not represent the real situation. Compare simulations side by side as both real and initialised bunches propagate further, see if any deviations occur or if the bunch I set up is actually a fair approximation (compare energy, particle number etc.)

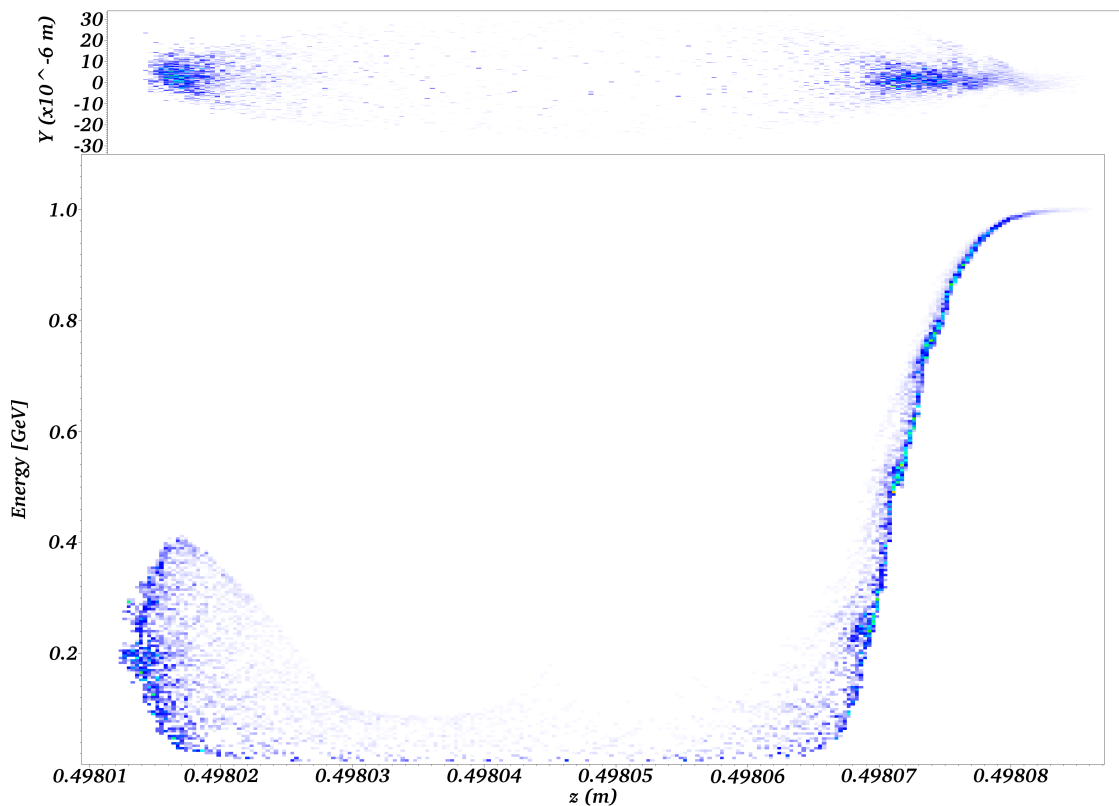
4.3.2 Introduction of co-propagating laser

- Results with respect to laser intensity/amplitude/wavelength as well as distance from bunch.



4. Simulation tests





5

Ongoing and future work

Having constructed the necessary computational framework for simulating the hybrid beam dump scheme we can now investigate the feasibility of this scheme and proceed to work out the details of the bunch-laser interaction. This will include investigating and optimizing the distance at which the laser is introduced, the spatial separation between the bunch and the the laser, the intensity and pulse length of the laser and effects caused by the difference in phase velocity between the bunch and the laser.

Once the details of the hybrid scheme has been investigated and a desirable approach has been determined we should proceed by high resolution simulations to verify that that the scheme works. As we have seen in section XXX the effect of insufficiently high simulation resolution can yield wildly different outcomes, as small effects can become amplified or neglected, in comparison to higher resolution runs. Consequently, in order to obtain reliable results from our simulations it is crucial to investigate the parameters that determine the resolution of the simulation. These include:

- The number of grid points: where a finer grid will increase the spatial resolution by having the macro-particles in adjacent grid cells be closer together, thus allowing the distribution of the plasma and bunch electrons to be more accurately modelled. This however comes at the cost of longer computational time.
- The number of macro particles in each grid cell: this has the same effect as using a finer grid by allowing the contents of grid cells to more accurately describe the distribution of micro-particles in those cells, since if only one macroparticle was used in a cell with electrons of varying energy and momentum that macroparticle would have to average these properties and thus remove the finer details of the plasma and bunch.
- The number of macro particles in the electron bunch: This number is crucial to accurately capture the small-scale effects on the bunch caused by the interaction with the plasma electrons.

How to establish these simulation parameters?

5. Ongoing and future work

We may divide the work on the hybrid scheme into three broad areas.

- Energy loss w.r.t bunch and plasma parameters
 - Eloss(bean width)
 - Eloss(length)
 - Eloss(n_p/n_b), where $n_p = n_p$ (beam width, beam length)
- Simulation parameters
 - Grid settings and resolution to avoid transverse instabilities
 - Minimise numerical noise using laser ramp
 - Accuracy vs. Computational cost
- Laser driver
 - Optimise laser parameters
 - * Time when introduced in simulation (at/before saturation)
 - * Distance from bunch
 - * Pulse length
 - * Intensity, wavelength
 - * Laser ramp
 - Further laser investigations
 - * Multiple consecutive laser pulses

6

Conclusion

Etiam velit esse cillum dolore eu fugiat nulla pariatur. Excepteur sint occaecat cupidatat non proident, sunt in culpa qui officia deserunt mollit anim id est laborum.

6. Conclusion

Bibliography

- [1] The Technical Design Report (TDR) of the European XFEL.
- [2] David T. Attwood, Anne Sakdinawat, and Linda Geniesse. *X-rays and extreme ultraviolet radiation : principles and applications.*
- [3] Z Insepov, J Norem, A Bross, A Moretti, Z Qian, Y Torun, D Huang, R A Rimmer, S Mhalilingam, and S Veitzer. A model of rf breakdown arcs. Technical report, 2008.
- [4] Pisin Chen, Toshiki Tajima, and Yoshiyuki Takahashi. Plasma Wakefield Acceleration for Ultrahigh-Energy Cosmic Rays. *Physical Review Letters*, 89(16):14–17, 2002.
- [5] T Tajima and J M Dawson. Laser Electron Accelerator. Technical Report 4, 1979.
- [6] E. Esarey, C. B. Schroeder, and W. P. Leemans. Physics of laser-driven plasma-based electron accelerators. *Reviews of Modern Physics*, 81(3):1229–1285, 2009.
- [7] Donna Strickland and Gerard Mourou. Compression of amplified chirped optical pulses. Technical report, 1985.
- [8] C. E. Clayton, K. A. Marsh, A. Dyson, M. Everett, A. Lal, W. P. Leemans, R. Williams, and C. Joshi. Ultrahigh-gradient acceleration of injected electrons by laser-excited relativistic electron plasma waves. *Physical Review Letters*, 70(1):37–40, jan 1993.
- [9] W P Leemans, B Nagler, A J Gonsalves, K Nakamura, C G R Geddes, E Esarey, C B Schroeder, and S M Hooker. GeV electron beams from a centimetre-scale accelerator.
- [10] Xiaoming Wang, Rafal Zgadzaj, Neil Fazel, Zhengyan Li, S. A. Yi, Xi Zhang, Watson Henderson, Y.-Y. Chang, R. Korzekwa, H.-E. Tsai, C.-H. Pai, H. Quevedo, G. Dyer, E. Gaul, M. Martinez, A. C. Bernstein, T. Borger, M. Spinks, M. Donovan, V. Khudik, G. Shvets, T. Ditmire, and M. C. Downer. Quasi-monoenergetic laser-plasma acceleration of electrons to 2-GeV. *Nature Communications*, 4(1):1988, dec 2013.
- [11] W.-P. Leemans, A.-J. Gonsalves, H.-S. Mao, K. Nakamura, C. Benedetti, C.-B. Schroeder, Cs. Tóth, J. Daniels, D.-E. Mittelberger, S.-S. Bulanov, J.-L. Vay, C.-G.-R. Geddes, and E. Esarey. Multi-GeV Electron Beams from Capillary-Discharge-Guided Subpetawatt Laser Pulses in the Self-Trapping Regime. *Physical Review Letters*, 113(24):245002, dec 2014.
- [12] Zhirong Huang, Yuantao Ding, and Carl B. Schroeder. Compact X-ray Free-Electron Laser from a Laser-Plasma Accelerator Using a Transverse-Gradient Undulator. *Physical Review Letters*, 109(20):204801, nov 2012.
- [13] Preliminary Conceptual Design Report for the FACET-II Project at SLAC National Accelerator Laboratory. Technical report.
- [14] E. Adli, A. Ahuja, O. Apsimon, R. Apsimon, A. M. Bachmann, D. Barrientos, F. Batsch, J. Bauche, V. K. Berglyd Olsen, M. Bernardini, T. Bohl, C. Bracco, F. Braunmüller, G. Burt,

- B. Buttenschön, A. Caldwell, M. Cascella, J. Chappell, E. Chevallay, M. Chung, D. Cooke, H. Damerau, L. Deacon, L. H. Deubner, A. Dexter, S. Doebert, J. Farmer, V. N. Fedosseev, R. Fiorito, R. A. Fonseca, F. Friebel, L. Garolfi, S. Gessner, I. Gorgisyan, A. A. Gorn, E. Grana-dos, O. Grulke, E. Gschwendtner, J. Hansen, A. Helm, J. R. Henderson, M. Hüther, M. Ibison, L. Jensen, S. Jolly, F. Keeble, S. Y. Kim, F. Kraus, Y. Li, S. Liu, N. Lopes, K. V. Lotov, L. Maricalva Brun, M. Martyanov, S. Mazzoni, D. Medina Godoy, V. A. Minakov, J. Mitchell, J. C. Molendijk, J. T. Moody, M. Moreira, P. Muggli, E. Öz, C. Pasquino, A. Pardons, F. Peña Asmus, K. Pepitone, A. Perera, A. Petrenko, S. Pitman, A. Pukhov, S. Rey, K. Rieger, H. Ruhl, J. S. Schmidt, I. A. Shalimova, P. Sherwood, L. O. Silva, L. Soby, A. P. Sosedkin, R. Speroni, R. I. Spitsyn, P. V. Tuev, M. Turner, F. Velotti, L. Verra, V. A. Verzilov, J. Vieira, C. P. Welsch, B. Williamson, M. Wing, B. Woolley, and G. Xia. Acceleration of electrons in the plasma wakefield of a proton bunch. *Nature*, 561(7723):363–367, 2018.
- [15] G Schrgder, U Jansson, R Jung, G R Stevenson, and E B Vossenberg. The LEP Beam Dumping System. pages 2429–2431.
- [16] Polepalle Satyamurthy, Pravin Rai, Vikas Tiwari, Kiran Kulkarni, John Amann, Raymond G. Arnold, Dieter Walz, Andrei Seryi, Tristan Davenne, Ottone Caretta, Chris Densham, and Robert B. Appleby. Design of an 18 MW vortex flow water beam dump for 500 GeV electrons/positrons of an international linear collider. *Nuclear Instruments and Methods in Physics Research, Section A: Accelerators, Spectrometers, Detectors and Associated Equipment*, 679:67–81, 2012.
- [17] D Schumann, J Neuhausen, J Eikenberg, M Rüthi, M Wohlmuther, P W Kubik, H.-A Synal, V Alfimov, G Korschinek, G Rugel, and Th Faestermann. Radiochemical analysis of a copper beam dump irradiated with high-energetic protons. *Radiochim. Acta*, 97:123–131, 2009.
- [18] A Leuschner and K Tesch. The residual radioactivity of a water-copper beam dump for the TESLA Test Facility. Technical report, 1998.
- [19] H. C. Wu, T. Tajima, D. Habs, A. W. Chao, and J. Meyer-ter Vehn. Collective deceleration: Toward a compact beam dump. *Physical Review Special Topics - Accelerators and Beams*, 13(10):1–8, 2010.
- [20] Kieran Hanahoe, Guoxing Xia, Mohammad Islam, Yangmei Li, Öznur Mete-Apsimon, Bernhard Hidding, and Jonathan Smith. Simulation study of a passive plasma beam dump using varying plasma density. *Physics of Plasmas*, 24(2), 2017.
- [21] A. Bonatto, C. B. Schroeder, J. L. Vay, C. G.R. Geddes, C. Benedetti, E. Esarey, and W. P. Leemans. Passive and active plasma deceleration for the compact disposal of electron beams. *Physics of Plasmas*, 22(8), 2015.
- [22] John M Dawson. Electron Oscillations in a Cold Plasma. Technical Report 2, 1959.
- [23] Spencer J Gessner. DEMONSTRATION OF THE HOLLOW CHANNEL PLASMA WAKEFIELD ACCELERATOR A DISSERTATION SUBMITTED TO THE DEPARTMENT OF PHYSICS AND THE COMMITTEE ON GRADUATE STUDIES OF STANFORD UNIVERSITY IN PARTIAL FULFILLMENT OF THE REQUIREMENTS FOR THE DEGREE OF DOCTOR OF PHIL. Technical report, 2016.
- [24] John David Jackson. Jackson - Classical Electrodynamics (3rd Ed.).pdf, 1962.
- [25] T Katsouleas, S Wilks, P Chen, J M Dawson, and J J Su. BEAM LOADING IN PLASMA ACCELERATORS. Technical report, 1987.

- [26] S Vaganian and H Henke. THE PANOFSKY-WENZEL THEOREM AND GENERAL RELATIONS FOR THE WAKE POTENTIAL. Technical report, 1995.
- [27] Francesco Mira and Thesis Advisor. Self Injection of High Brightness electron beams via Wakefield Ionization in beam-driven Plasma Acceleration. (October), 2017.
- [28] A. Bonatto, C. B. Schroeder, J. L. Vay, C. R. Geddes, C. Benedetti, E. Esarey, and W. P. Leemans. Compact disposal of high-energy electron beams using passive or laser-driven plasma decelerating stage. *AIP Conference Proceedings*, 1777(1):0–5, 2016.
- [29] K Schmid and L Veisz. Supersonic gas jets for laser-plasma experiments. *Citation: Review of Scientific Instruments*, 83:53304, 2012.

Bibliography

A

Appendix: Input decks